Ultrafast quantum nondemolition measurements based on a diamond-shaped artificial atom

I. Diniz, E. Dumur, O. Buisson, and A. Auffèves
Institut Néel, CNRS–Université Joseph Fourier, Boîte Postale 166, 38042 Grenoble Cedex 9, France
(Received 18 July 2012; published 28 March 2013)

We propose a quantum nondemolition (QND) readout scheme for a superconducting artificial atom coupled to a resonator in a circuit QED architecture, for which we estimate a very high measurement fidelity without Purcell effect limitations. The device consists of two transmons coupled by a large inductance, giving rise to a diamond-shaped artificial atom with a logical qubit and an ancilla qubit interacting through a cross-Kerr-like term. The ancilla is strongly coupled to a transmission line resonator. Depending on the qubit state, the ancilla is resonantly or dispersively coupled to the resonator, leading to a large contrast in the transmitted microwave signal amplitude. This original method can be implemented with a state-of-the-art Josephson parametric amplifier, leading to QND measurements in a few tens of nanoseconds with fidelity as large as 99.9%.

DOI: 10.1103/PhysRevA.87.033837 PACS number(s): 42.50.Pq, 03.65.Ta, 85.25.−j

I. INTRODUCTION

Superconducting circuits have demonstrated in the last decade their high ability to perform coherent quantum experiments [1,2]. Relaxation T_1 and coherence T_2 times are continuously increasing [3]. In addition, these quantum systems benefit from very strong coupling with the electromagnetic field and potential scalability. Finally, the circuit parameters that define the quantum dynamics are tunable and adjustable on demand, which makes them very promising candidates to process quantum information on a chip. In this framework, the ability to perform ultrafast single-shot readout of a quantum bit is highly desirable. Up to now, high one-shot fidelity was obtained by switching quantum measurements using an escape process [4], the intrinsic drawback of this method being its destructiveness. Quantum nondemolition (QND) measurements are performed by coupling the qubit dispersively to a resonator [5]. The qubit acts as a state-dependent refractive index that shifts the cavity frequency, and the measurement is performed by probing the resonator with an external microwave. QND character is preserved as long as one remains in the dispersive regime, keeping the photon population $\bar{n}$ of the resonator below a critical value [6] and also limiting the incident power. Low-temperature amplifiers thus have to be used to reach high fidelity. On the other hand, using a nonlinear resonator and bifurcation [7,8] or Jaynes-Cummings nonlinearity [9] allows us to reach one-shot high-fidelity readout, but at the price of lower QND fidelity. Thanks to recent advances in parametric amplification using Josephson-junction circuits [10–12], single-shot readout has been demonstrated, allowing us to observe quantum jumps in superconducting artificial atoms [13], high-fidelity readout [14–16], and ever-persisting Rabi oscillations [17]. However, this measurement scheme still requires several hundred nanoseconds of measurement time to reach high fidelity. Consequently, further improvements are necessary in order to reach very high fidelity measurements in a few tens of nanoseconds. New quantum measurement protocols inspired by ion traps and quantum optics were recently proposed with this purpose [18,19].

Here we propose an original method to realize ultrafast QND measurements of a qubit with large resonator linewidth and measurement bandwidth while preserving high fidelity. Our system is a resonator coupled to a four-level diamond-shaped atom, which can be seen as two qubits coupled by crossed Kerr interaction. In this picture, the first qubit is the one we read out, while the second qubit plays the role of an ancilla whose frequency depends on the first qubit state. The resonator is not coupled to the qubit, only to the ancilla. This huge difference with respect to previous experiments induces important consequences for the qubit and for the resonator properties. First, the Purcell effect between the qubit and the cavity is absent, and the readout performance is independent from the detuning between the qubit and the resonator. Second, the present proposal allows us to eliminate the harsh constraint on the amplification and resonator bandwidth, leading to fast, one-shot, high-fidelity QND readout of our qubit even with present-day amplifier technology.

II. QND READOUT SCHEME ON DIAMOND-SHAPED ARTIFICIAL ATOM

We exemplify hereafter this method with a diamond-shaped artificial atom consisting of two transmons coupled by a large inductance. The system under study here is pictured in Fig. 1, in which the resonator is schematized by a coplanar waveguide resonator, but our result can be applied to three-dimensional (3D) cavities or lumped-element resonators. The Josephson energy $E_J = \Phi_0 I_c/2\pi$ and the charging energy $E_c = e^2/2C$, with I_c and C being the critical current and the capacitance per junction, are fixed to verify the typical ratio $E_J/E_c \approx 50$ of the transmons limiting the decoherence effects [20]. Such devices can be described by an anharmonic oscillator with two degrees of freedom. Its quantum description is the same as the one performed in Ref. [21] for a dc superconducting quantum interference device (SQUID) in the particular case of zero-current bias or in Refs. [22,23] for two transmons coupled by a SQUID. It gives rise to two orthogonal modes, the symmetric and antisymmetric modes [21]. When the anharmonicity is strong enough, we can consider just the first two levels of the two modes. The system is then reduced to two coupled two-level systems. The two first quantum states of the symmetric mode, $|g\rangle$ and $|e\rangle$, provide the logical qubit σ_z^{qb}. The second two-level system corresponds to the two first quantum states of the antisymmetric mode, and it will be used as an ancilla σ_z^a for the quantum measurement. In the absence

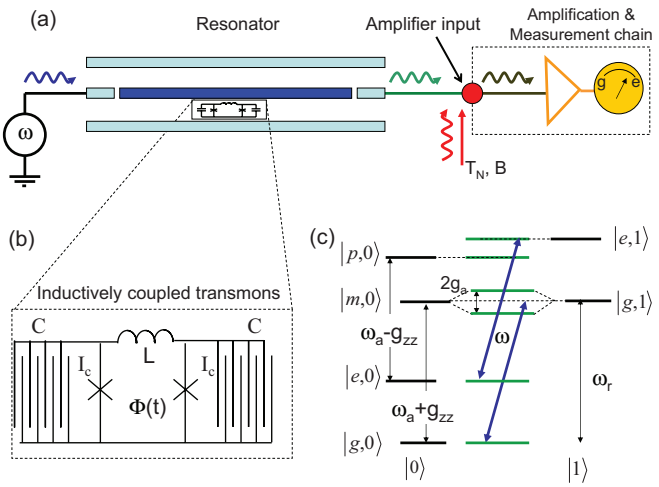

FIG. 1. (Color online) (a) Schematic circuit for a fast QND readout. The incident microwave signal of frequency ω is transmitted through the resonator coupled to the superconducting artificial atom. The transmitted signal is amplified and homodyne detected. The noise amplifier is illustrated by an additional microwave source at the amplifier input. (b) The artificial atom, realized by two transmons coupled by a large inductance. (c) Energy spectrum of the uncoupled (left and right) and dressed (center) diamond-shaped artificial atom-resonator states when $\omega_r = \omega_a + g_{zz}$. The blue (gray) arrows indicate the injected microwave frequency when $\omega = \omega_r$.

of coupling between the two modes, the transition frequencies of the qubit and ancilla are given by ω_{qb} and ω_a, respectively. Hereafter we restrict our study to the working point given by zero-flux bias, which constitutes an optimal point for the artificial atom. The coupling between the two systems is reduced to a longitudinal interaction term $\sigma_z^{qb}\sigma_z^a$ with a strength given by $\hbar g_{zz} = E_c/(\sqrt{1+2E_L/E_J})$ [24], where $E_L = (\Phi_0/2\pi)^2/L$, with L being the SQUID inductance. This term can be viewed as an analog of a cross-Kerr term between the two quantum systems, leading to a conditional energy transition of the ancilla which depends on the quantum state of the qubit $|g\rangle$ and $|e\rangle$. The respective frequencies of the transitions $|g\rangle \to |m\rangle$ and $|e\rangle \to |p\rangle$ are $\hbar(\omega_a + g_{zz})$ and $\hbar(\omega_a - g_{zz})$. The artificial atom inside a coplanar resonator is described by the following Hamiltonian, written in the rotating-wave approximation:

$$H_{\text{free}} = \hbar\omega_{qb}\sigma_z^{qb}/2 + \hbar(\omega_a - g_{zz}\sigma_z^{qb})\sigma_z^a/2 + \hbar\omega_r(a^\dagger a + 1/2) - i\hbar g_a(a\sigma_+^a - a^\dagger\sigma_-^a). \quad (1)$$

The first three terms describe the artificial atom, and the fourth describes the resonator of frequency ω_r. In the following we choose the frequency condition between the resonator and the ancilla: $\omega_r = \omega_a + g_{zz}$. The last term couples the resonator and the ancilla when the artificial atom is localized at the center of the resonator. Indeed, at this particular place, the quantum fluctuation of the flux is maximal, and the voltage fluctuations are reduced to zero. Because of a zero-flux bias working point, the qubit is not affected by flux fluctuations, leading to zero coupling between the resonator and the qubit. This way, σ_z^{qb} commutes with the Hamiltonian of the system, ensuring the nondestructive character of the measurement whatever the number of photons in the resonator.

III. TRANSMITTED MICROWAVE SIGNAL AMPLITUDE

To describe the transmission properties of the cavity as a function of the qubit state, we write a closed set of differential equations from Eq. (1), describing the time evolution of the system operators in the Heisenberg picture. These are deduced from input-output equations established in the case of a transmitting cavity as in [25]. We define the external fields b_{in} (injected microwave field), b_r (reflected field), and b_t (transmitted field), which lead to the usual input-output equations: $b_r = b_{in} + i\sqrt{\kappa}a$ and $b_t = i\sqrt{\kappa}a$, where κ is the resonator coupling to external transmission line modes. As we consider an overcoupled cavity, we neglect the internal losses of the resonator, and thus κ entirely defines the resonator linewidth. The qubit energy relaxation and dephasing times are assumed to be very long compared to the resonator relaxation time ($\kappa T_1 \gg 1$ and $\kappa T_2 \gg 1$). The Heisenberg equations are written in the frame rotating at the frequency ω of the probe, yielding

$$\begin{aligned}
\dot{\sigma_z^a} &= -2g_a(\sigma_+^a a + \sigma_-^a a^\dagger)\,,\\
\dot{\sigma_-^a} &= -i(\omega_r - \omega + \delta_j)\sigma_-^a + g_a\sigma_z^a a\,,\\
\dot{\sigma_-^{qb}} &= -i\left(\omega_{qb} - g_{zz}\sigma_z^a\right)\sigma_-^{qb}\,,\\
\dot{a} &= -i(\omega_r - \omega)a - \kappa a + g_a\sigma_-^a + i\sqrt{\kappa}b_{in}\,,
\end{aligned} \quad (2)$$

where $\delta_j = -g_{zz}(1+\sigma_z^{qb})$ is the qubit-state-dependent shift and the index j defines the qubit state ($j = g$ or e). As expected from a QND measurement, the evolution preserves $\langle\sigma_z^{qb}\rangle$. We are interested in the transmission properties of this system in the steady-state regime established after a time much larger than $1/\kappa$. We adopt the semiclassical approach where the quantum correlations between atomic and field operators are neglected [25]. From now on we identify the operators with their average complex values, which could be measured in a homodyne experiment. The ratio $t(\omega) = \langle b_t\rangle/\langle b_{in}\rangle$ can be written in the steady-state regime as

$$t_j(\omega) = t_0(\omega)\left\{1 - \frac{1}{1+\frac{p}{p_s}}\left[1 - \frac{2i(\omega_r + \delta_j - \omega)}{\Gamma t_0(\omega)}\right]^{-1}\right\}, \quad (3)$$

where $\Gamma = 2g_a^2/\kappa$ and $t_0(\omega) = -[1 + i(\omega_r - \omega)/\kappa]^{-1}$ is the transmission of the empty resonator. We have introduced the drive power in units of photons per second, $p = \langle b_{in}^\dagger b_{in}\rangle$, and the saturation power p_s of the atom-cavity system reads $\frac{p_s}{\Gamma} = \frac{(\omega_r+\delta_j-\omega)^2}{\Gamma^2} + [\frac{(\omega_r-\omega)}{\Gamma}\frac{(\omega_r+\delta_j-\omega)}{\kappa} - 1/2]^2$.

The essence of the protocol is pictured in Fig. 2 in the linear regime when $p \ll p_s$. In this regime the transmission is given by $t_j(\omega) = [\frac{1}{t_0(\omega)} + \frac{i\Gamma}{2(\omega_r+\delta_j-\omega)}]^{-1}$. If the qubit is in state $|g\rangle$, $\delta_g = 0$, so that the ancilla qubit is resonant with the cavity mode and the transmission consists of two peaks located at $\pm g_a$ with respect to the frequency of the resonator. If the qubit is in state $|e\rangle$, $|\delta_e| = 2g_{zz}$, inducing a dispersive coupling between the resonator and the ancilla provided that $g_{zz} > g_a$. The transmission essentially consists of a single peak slightly shifted by $\delta_L = g_{zz}(\sqrt{1+g_a^2/g_{zz}^2} - 1)$ with respect to ω_r (see Fig. 2). Thus a change in the state of the qubit can now translate

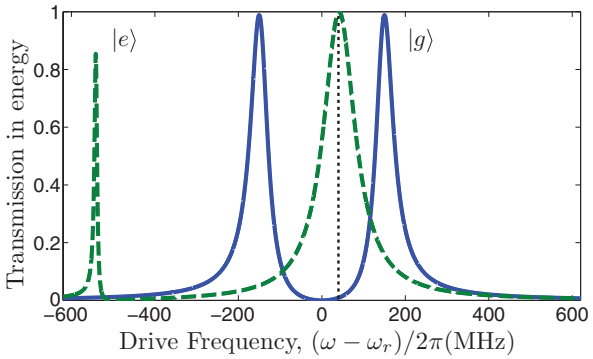

FIG. 2. (Color online) Transmission coefficient at low pump power for a microwave pulse injected in a resonator containing a diamond-shaped artificial atom. Blue solid curve: qubit state $|g\rangle$. Green dashed curve: qubit state $|e\rangle$. The frequency is centered on the bare cavity. We took $g_{zz}/2\pi = 250$ MHz, $g_a/2\pi = 150$ MHz, a cavity linewidth $\kappa/2\pi = 40$ MHz ($Q = 250$), and $p \ll p_s$. The black dotted line indicates the pump frequency $(\omega_r + \delta_L)/2\pi$.

into a switch from dispersive to resonant coupling between the resonator and the ancilla. This is evidenced by a visible displacement in the transmission peaks by a quantity g_a, which can be as high as 150 MHz, about two orders of magnitude higher than the usual dispersive ac Stark shift [13,14]. This strong effect allows an increase in the linewidth of the resonator while keeping a high-fidelity readout. Working with a low-Q cavity has important advantages. First, it drastically increases the total bandwidth of the circuit and, consequently, the readout speed. Moreover, for the same probe power, the average intracavity photon number is lower, preserving the lifetime and coherence time of the qubit [6]. The readout is performed by the injection of a short microwave pulse of power p at the frequency $(\omega_r + \delta_L)/2\pi$. Thus, the transmitted power depends on the state of the qubit, giving rise to two conditional output signals, $p_{t|j} = \langle b_t^\dagger b_t \rangle = |t_j|^2 p$. When p largely overcomes p_s, one recovers the transmission pattern $t_0(\omega)$ of the empty cavity, a signature of saturation [25] which limits the information on the qubit state.

IV. READOUT FIDELITY IN THE PRESENCE OF AMPLIFICATION NOISE

We now introduce the model to optimize the measurement scheme. The performance of the readout is usually quantified by two figures of merit, namely, their fidelity $\mathcal{F}$ and speed. Speed is high when the system can be measured frequently, the delay between two measurements being inferiorly bounded by their typical correlation time τ_c. τ_c is related to the inertia of the circuit since the resonator imposes $\tau_c > \kappa^{-1}$. Fidelity and correlation time depend on two independent parameters to optimize. First, the resonator linewidth should be narrow enough to give a large contrast between the two transmission patterns ($\kappa < g_a, g_{zz}$) but large enough to allow a large transmitted signal $p_{t|j} = \bar{n}_j \kappa$ and therefore high-speed qubit readout for a given photon number $\bar{n}_j$ inside the resonator. In the same way, the driving power p should be sufficiently low to avoid the saturation of the ancilla $p \ll p_s$ but high enough to have a large $p_{t|j}$.

In a typical circuit QED experiment, microwave photons are amplified before being sent through a homodyne detection scheme and digitalized within a short time interval τ, which is usually equal to τ_c. For our purpose, we shall consider the field at the entrance of the amplifying chain. The chain is modeled by a perfect amplifier [11] radiating a white thermal field of effective temperature T_N at the input of the amplifier. This noise temperature ranges from a few hundreds of mK for the recent generation of quantum-limited devices [12,15] to 4–10 K for commercial devices. The total noise power $\mathcal{N} = (k_B T_N/\hbar\omega)B$, in units of photons per second, is given by Johnson-Nyquist noise [26], where B is the bandwidth of the amplifier, imposing an additional lower band on the correlation time $\tau_c > B^{-1}$. Consequently, high-speed measurements are obtained at the price of increased bandwidth and noise power $\mathcal{N}$.

The estimation of the readout fidelity is based on the photon number distributions $\mathbf{P}(n|j)$ conditioned to the qubit j, which we computed using the Glauber-Sudarshan P representation [27]. In our case, this simply corresponds to the P representation of a thermal field of temperature T_N displaced by a coherent field of amplitude $\sqrt{p_{t|j}}$. Thus we can readily calculate the generating function [28] for the photon statistics, from which we extract the coefficients

$$\mathbf{P}(n|j) = \frac{\mathcal{N}^n \tau^n}{(1+\mathcal{N}\tau)^{n+1}} \exp\left(\frac{-\tau\, p_{t|j}}{1+\mathcal{N}\tau}\right) L_n\left(\frac{-p_{t|j}\,/\mathcal{N}}{1+\mathcal{N}\tau}\right), \tag{4}$$

where L_n is the nth-order Laguerre polynomial.

The histograms plotted in Fig. 3 clearly show how the amplification noise has a large effect on the statistics of the counts associated with each of the qubit states. As expected, the noise power increases with noise temperature [Fig. 3(a) vs Fig. 3(c) and Fig. 3(b) vs Fig. 3(d)], degrading the fidelity. By increasing the integration time, one can regain fidelity [Fig. 3(a) vs Fig. 3(b) and Fig. 3(c) vs Fig. 3(d)]. As a matter of fact, it increases the signal, but it also allows one to operate with a lower bandwidth, reducing the noise power. We expect this protocol to yield a fidelity as high as 90% with a commercial

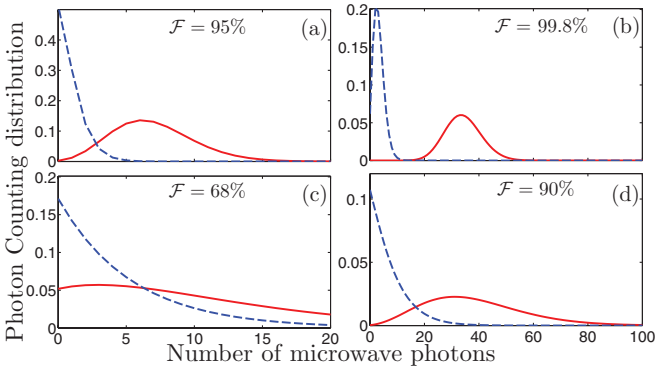

FIG. 3. (Color online) Photon distribution at the entrance of the amplifier as function of the noise temperature T_N and acquisition time τ. Histograms $\mathbf{P}(n|e)$ (red solid curve) and $\mathbf{P}(n|g)$ (blue dashed curve) with $\kappa = 40$ MHz and $p = 1$ photon/ns. (a) $T_N = 140$ mK, $\tau = 10$ ns, $B = 50$ MHz; (b) $T_N = 140$ mK, $\tau = 50$ ns, $B = 10$ MHz; (c) $T_N = 4$K, $\tau = 10$ ns, $B = 50$ MHz; (d) $T_N = 4$ K, $\tau = 50$ ns, $B = 10$ MHz

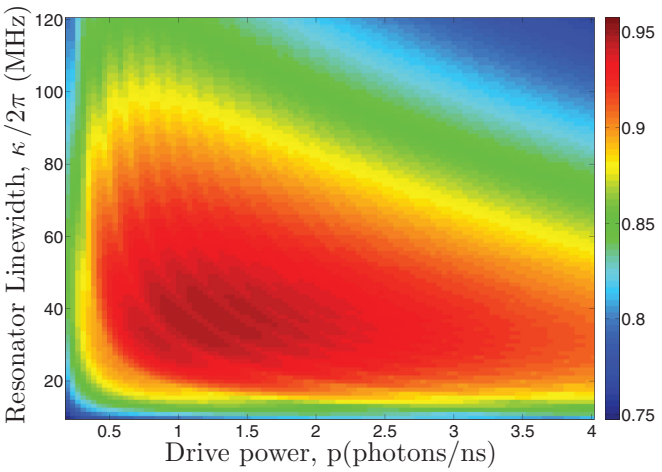

FIG. 4. (Color online) Single-measurement fidelity for a state-of-the-art amplifier ($T_N = 140$ mK) and an acquisition time $\tau = 10$ ns vs drive power p in units of photons/ns and resonator linewidth κ. The optimal value of $\mathcal{F} = 95\%$ is reached for a broad range around $\kappa = 40$ MHz and $p = 1$ photon/ns.

amplifier, within a typical time of $\tau = 50$ ns. An integration as short as $\tau = 60$ ns should be enough to reach 99.9% with a state-of-the-art amplifier with $T_N = 140$ mK [15].

Figure 4 shows the optimization of the fidelity as a function of the resonator linewidth and probe power. The digitization time $\tau = 10$ ns has been chosen, which is compatible with a bandwidth $B = 50$ MHz. A fidelity $\mathcal{F} = 95\%$ can be reached with a resonator linewidth $\kappa = 40$ MHz and very small pumping power, corresponding to $\bar{n} = 1.8$ photons. This fidelity corresponds to up-to-date results obtained in the dispersive measurement scheme with the same amplifier [13,15] but allows a much faster acquisition time. Indeed, in dispersive-based readout schemes the dynamics is slow because of the inertia imposed by the resonator of linewidth $\kappa \sim 5$ MHz, inducing a typical correlation time of $\tau_c = 100$ ns. With our scheme, using a low-temperature amplifier allows a drastic increase in the bandwidth and readout speed. This enables a projective measurement of the qubit to be performed on a time scale much shorter than the recently measured relaxation time, $T_1 = 50$ μs [3]. This scheme opens the path to the observation of quantum jumps in circuit QED with a very high temporal resolution, comparable to the performances achieved in recent experiments performed with Rydberg atoms [29], where the system is typically measured 10^3 times before undergoing a quantum jump.

V. CONCLUSION

In conclusion we propose a readout scheme based on a superconducting diamond-shaped artificial atom which contains a logical qubit strongly coupled to an ancilla qubit by a cross-Kerr term. We predict fast high-fidelity QND readout of the transmon qubit with a commercial amplifier. Using a quantum-limited amplifier, 60 ns readout time and 99.9% fidelity are predicted. This original method overcomes the current readout limitation of the superconducting qubits dispersively coupled to a resonator. In addition the Purcell effect between the logical qubit and cavity is absent. As a side effect the intracavity population is minimal, $\bar{n} = 1.8$, for the optimal parameters, minimizing any adverse effect on the qubit coherence properties. This opens the possibility of monitoring quantum jumps of the qubit with very high temporal resolution [29], of generating nonclassical states [30], or of implementing quantum error correction codes [31] using closed feedback loops.

ACKNOWLEDGMENTS

The authors gratefully thank N. Roch, P. Bertet, P. Milman, A. K. Feofanov, and I. M. Pop for useful discussions. This work was supported by the European SOLID and the ANR-NFSC QuExSuperC projects, Nanosciences Foundation of Grenoble, and CAPES.

[1] A. Korotkov, Quantum Inf. Process. **8**, 51 (2009).
[2] J. Clarke and F. K. Wilhelm, Nature (London) **453**, 1031 (2008).
[3] H. Paik, D. I. Schuster, Lev S. Bishop, G. Kirchmair, G. Catelani, A. P. Sears, B. R. Johnson, M. J. Reagor, L. Frunzio, L. I. Glazman, S. M. Girvin, M. H. Devoret, and R. J. Schoelkopf, Phys. Rev. Lett. **107**, 240501 (2011).
[4] E. Lucero, M. Hofheinz, M. Ansmann, R. C. Bialczak, N. Katz, M. Neeley, A. D. O'Connell, H. Wang, A. N. Cleland, and J. M. Martinis, Phys. Rev. Lett. **100**, 247001 (2008).
[5] A. Wallraff, D. I. Schuster, A. Blais, L. Frunzio, J. Majer, M. H. Devoret, S. M. Girvin, and R. J. Schoelkopf, Phys. Rev. Lett. **95**, 060501 (2005).
[6] M. Boissonneault, J. M. Gambetta, and A. Blais, Phys. Rev. A **79**, 013819 (2009).
[7] I. Siddiqi, R. Vijay, M. Metcalfe, E. Boaknin, L. Frunzio, R. J. Schoelkopf, and M. H. Devoret, Phys. Rev. B **73**, 054510 (2006).
[8] F. Mallet, F. R. Ong, A. Palacios-Laloy, F. Nguyen, P. Bertet, D. Vion, and D. Esteve, Nat. Phys. **5**, 791 (2009).
[9] M. D. Reed, L. DiCarlo, B. R. Johnson, L. Sun, D. I. Schuster, L. Frunzio, and R. J. Schoelkopf, Phys. Rev. Lett. **105**, 173601 (2010).
[10] A. A. Clerk, M. H. Devoret, S. M. Girvin, Florian Marquardt, and R. J. Schoelkopf, Rev. Mod. Phys. **82**, 1155 (2010).
[11] N. Bergeal, F. Schackert, M. Metcalfe, R. Vijay, V. E. Manucharyan, L. Frunzio, D. E. Pobrer, R. J. Schoelkopf, S. M. Girvin, and M. H. Devoret, Nature (London) **465**, 64 (2010).
[12] N. Roch, E. Flurin, F. Nguyen, P. Morfin, P. Campagne-Ibarcq, M. H. Devoret, and B. Huard, Phys. Rev. Lett. **108**, 147701 (2012).
[13] R. Vijay, D. H. Slichter, and I. Siddiqi, Phys. Rev. Lett. **106**, 110502 (2011).
[14] D. Riste, J. G. van Leeuwen, H. S. Ku, K. W. Lehnert, and L. DiCarlo, Phys. Rev. Lett. **109**, 050507 (2012).
[15] J. E. Johnson, C. Macklin, D. H. Slichter, R. Vijay, E. B. Weingarten, J. Clarke, and I. Siddiqi, Phys. Rev. Lett. **109**, 050506 (2012).

[16] M. Hatridge, S. Shankar, M. Mirrahimi, F. Schackert, K. Geerlings, T. Brecht, K. M. Sliwa, B. Abdo, L. Frunzio, S. M. Girvin, R. J. Schoelkopf, and M. H. Devoret, Science **339**, 178 (2013).

[17] R. Vijay, C. Macklin, D. H. Slichter, S. J. Weber, K. W. Murch, R. Naik, A. N. Korotkov, and I. Siddiqi, Nature (London) **490**, 77 (2012).

[18] B. G. U. Englert, G. Mangano, M. Mariantoni, R. Gross, J. Siewert, and E. Solano, Phys. Rev. B **81**, 134514 (2010).

[19] S. Kumar and D. P. Di Vincenzo, Phys. Rev. B **82**, 014512 (2010).

[20] J. Koch, T. M. Yu, J. Gambetta, A. A. Houck, D. I. Schuster, J. Majer, A. Blais, M. H. Devoret, S. M. Girvin, and R. J. Schoelkopf, Phys. Rev. A **76**, 042319 (2007).

[21] F. Lecocq, J. Claudon, O. Buisson, and P. Milman, Phys. Rev. Lett. **107**, 197002 (2011).

[22] Y. Hu, G.-Q. Ge, S. Chen, X.-F. Yang, and Y.-L. Chen, Phys. Rev. A **84**, 012329 (2011).

[23] L. Neumeier, M. Leib, and M. J. Hartmann, arXiv:1211.7215.

[24] F. Lecocq, I. M. Pop, I. Matei, E. Dumur, A. K. Feofanov, C. Naud, W. Guichard, and O. Buisson, Phys. Rev. Lett. **108**, 107001 (2012).

[25] A. Aufféves-Garnier, C. Simon, J. M. Gerard, and J. P. Poizat, Phys. Rev. A **75**, 053823 (2007).

[26] J. B. Johnson, Phys. Rev. **32**, 97 (1928); H. Nyquist, *ibid*. **32**, 110 (1928).

[27] R. Glauber, Phys. Rev. **131**, 2766 (1963).

[28] L. Mandel and E. Wolf, *Optical Coherence and Quantum Optics* (Cambridge University Press, Cambridge, 1995).

[29] S. Gleyzes, S. Kuhr, C. Guerlin, J. Bernu, S. Deléglise, U. B. Hoff, M. Brune, J.-M. Raimond, and S. Haroche, Nature (London) **446**, 297 (2007).

[30] X. Zhou, I. Dotsenko, B. Peaudecerf, T. Rybarczyk, C. Sayrin, S. Gleyzes, J. M. Raimond, M. Brune, and S. Haroche, Phys. Rev. Lett. **108**, 243602 (2012).

[31] M. A. Nielsen and I. L. Chuang, *Quantum Computation and Quantum Information* (Cambridge University Press, Cambridge, 2000).